Dissecting the Molecular Mechanism of Apoptosis during Photothermal Therapy Using Gold Nanoprisms

Marta Pérez-Hernández,[†,‡,¶] Pablo del Pino,[*,†,§,¶] Scott G. Mitchell,[†] María Moros,[†] Grazyna Stepien,[†] Beatriz Pelaz,[#] Wolfgang J. Parak,[#,§] Eva M. Gálvez,[∥,‡] Julián Pardo,[*,†,‡,⊥] and Jesús M. de la Fuente[*,†,▽,⊗]

[†]Instituto Universitario de Nanociencia de Aragón (INA), Universidad de Zaragoza, 50018 Zaragoza, Spain, [‡]Aragón Health Research Institute (IIS Aragón), Biomedical Research Centre of Aragón (CIBA), 50009 Zaragoza, Spain, [§]CIC biomaGUNE, Paseo Miramon 182, 20009 San Sebastián, Spain, [⊥]Fundacion ARAID, 50018 Zaragoza, Spain, [∥]Instituto de Carboquímica, ICB-CSIC, 50018 Zaragoza, Spain, [#]Faculty of Physics, Philipps-Universität Marburg, 35037 Marburg, Germany, [▽]Instituto de Ciencia de Materiales de Aragón (ICMA), CSIC-Universidad de Zaragoza, C/Pedro Cerbuna 12, 50009 Zaragoza, Spain, and [⊗]Institute NanoBiomedicine and Engineering, Shanghai Jiao Tong University, Dongchuan Road 800, 200240 Shanghai, PR China. [¶]M.P.-H. and P.d.P. contributed equally.

ABSTRACT The photothermal response of plasmonic nanomaterials can be exploited for a number of biomedical applications in diagnostics (biosensing and optoacoustic imaging) and therapy (drug delivery and photothermal therapy). The most common cellular response to photothermal cancer treatment (ablation of solid tumors) using plasmonic nanomaterials is necrosis, a process that releases intracellular constituents into the extracellular milieu producing detrimental inflammatory responses. Here we report the use of laser-induced photothermal therapy employing gold nanoprisms (NPRs) to specifically induce apoptosis in mouse embryonic fibroblast cells transformed with the SV40 virus. Laser-irradiated "hot" NPRs activate the intrinsic/mitochondrial pathway of apoptosis (programmed cell death), which is mediated by the nuclear-encoded proteins Bak and Bax through the activation of the BH3-only protein Bid. We confirm that an apoptosis mechanism is responsible by showing how the NPR-mediated cell death is dependent on the presence of caspase-9 and caspase-3 proteins. The ability to selectively induce apoptotic cell death and to understand the subsequent mechanisms provides the foundations to predict and optimize NP-based photothermal therapy to treat cancer patients suffering from chemo- and radioresistance.

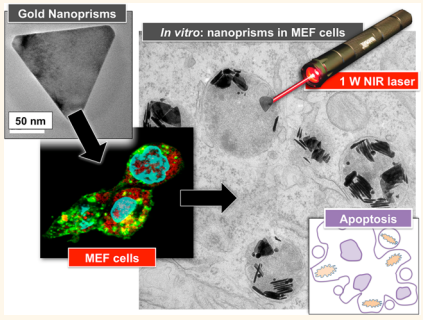

KEYWORDS: gold nanoparticles · nanoprism · NIR window · photothermal · apoptosis · mitochondrial pathway · Bcl-2 family

The photothermal effect relies in the ability of plasmonic materials to convert absorbed light into heat. The photothermal response of these materials has been explored for many relevant life science applications including photothermal therapy,[1,2] drug delivery,[3,4] photothermal,[5,6] and optoacoustic imaging,[2,7] as well as biosensing.[8,9] Photothermal cancer treatment (ablation of solid tumors) using gold nanoparticles has reached the stage of clinical trials;[1] while optoacoustic tomography (PAT) is in preclinical stage.[10] The impact of these techniques on fundamental research in life science and clinical care are expected to be groundbreaking.

During the last two decades, the number of reports on thermoplasmonics toward applications in life science has been overwhelming, particularly with regard to materials development and cancer treatment.[11] Considerable research efforts have focused on the design of plasmonic materials, which can produce heat upon excitation by near-infrared (NIR) light, since biological tissues display a limited absorption of light from this range of the EM spectrum, the so-called NIR-biological window.[12] A vast array of plasmonic materials with different compositions (gold, silver, copper, graphene, copper selenide, carbon nanotubes, *etc.*), structures (solid or hollow), shapes (nanorods, pseudospherical, triangular prisms, *etc.*) and surface coatings (polymeric coatings, peptides, carbohydrates, hydrophobic/hydrophilic patterned, *etc.*) are available for these purposes. However, the intrinsic physicochemical properties of gold nanoshells,[13] nanorods[14] and nanocages[15] offer favorable stability and high heating efficiency combined with a wide variety of synthetic methods to produce such nanostructures.

* Address correspondence to jmfuente@unizar.es, pardojim@unizar.es, pdelpino@cicbiomagune.es.

Received for review September 26, 2014 and accepted December 10, 2014.

Published online December 10, 2014
10.1021/nn505468v

Other shapes such as nanoprisms and more complex nanoarchitectures involving coupling between materials are expected to be more efficient nanoheaters.[16] We recently reported a high-yielding synthetic method for producing anisotropic gold nanoprisms (NPRs) in the absence of highly toxic reagents.[17] The polymeric surface of these NPRs can be modified with molecules of biological relevance to enhance cell internalization and specificity. We have shown how these particular NPRs can be used as highly efficient nanoheaters for ablation of cells *in vitro*,[17] photoactive agents for *in vivo* optoacoustic multispectral tomography,[7] as well as thermoresponsive materials for biosensing applications.[9]

Plasmonic nanoparticle-mediated photothermal therapy typically involves delivery of NPs to the tumor cells followed by irradiation to produce a localized elevation in temperature.[18] A limited number of studies have proposed that apoptosis is induced in cells during photothermal therapy using different types of NPs.[19−21] However, most of those works did not explore in detail if cell death was eminently apoptotic and still necrosis is the most common cellular response during tumor ablation carried out *via* NP-mediated photothermal therapy.[22−24] Since uncontrolled necrosis typically leads to the release of intracellular constituents into the extracellular milieu, the resulting inflammatory responses that are induced may produce a detrimental knock-on effect by damaging adjacent tissues, inducing tumor growth, and so forth.[25]

Apoptosis is essential for ontogenetic development as well as adult tissue remodeling and helps to eliminate damaged, infected, or tumoral cells.[26] This mechanism is characterized by oligonucleosomal DNA fragmentation, chromatin condensation, mitochondrial dysfunction, and translocation of the phosphatidylserine phospolipid (PS) to the outer part of the plasmatic cell membrane. In contrast to necrosis, membrane integrity is preserved during apoptosis due to the presence of a number of molecules known as "eat me" signals in the plasma membrane of dying cells.[27] Thanks to these signals, apoptotic bodies are rapidly cleared by phagocytic cells including macrophages, epithelial and dendritic cells, avoiding the detrimental effects of necrosis. Further, although apoptotic cell death also induces an inflammatory immune response, the mechanism and consequences of this reaction are rather different than during necrosis. For example, phagocytosis of apoptotic cells usually activates antitumoral immunity by a process known as T cell cross-priming.[28,29]

Two families of molecules are primarily responsible for regulating the apoptotic process: (a) a family of phylogenetically conserved heterodimeric cysteine proteases (caspases) divided into pro-inflammatory (caspase-1, -4 and -5), initiator (caspase-2, -8, -9 and -10) and executioner (caspase-3, -6 and -7) subsets,[30] and (b) a group of proteins known as the Bcl-2 family, consisting of pro-apoptotic (Bak, Bax, Bid, Bim, Noxa, PUMA *etc.*) or antiapoptotic (Bcl-2, Mcl-1, Bcl-X_L, *etc.*) proteins.[31] Both the caspases and the Bcl-2 families are connected through the mitochondrial apoptosis pathway. Activation of the pro-apoptotic members of the Bcl-2 family Bak and Bax, which is usually triggered by pro-apoptotic BH3-only members like Bid, Bim or PUMA, is associated with the loss of mitochondrial membrane potential and the release from the intermembrane space of molecules, including cytochrome c (cyt c). Cyt c, once released into the cytoplasm, interacts with Apaf-1, deoxyadenosine triphosphate (dATP) and pro-caspase 9, forming a complex termed apoptosome that facilitates the activation of downstream executioner caspases-3, -6 or -7, which are ultimately responsible for dismantling the cellular structure and inducing other features that are typical of apoptotic cell death.

As a response to external stimuli, both apoptosis and necrosis can occur independently, sequentially and simultaneously.[32] Indeed, the cellular response of cells or tissue containing plasmonic nanomaterials can be expected to be complex and will depend highly on the quantity that is internalized as well as on the amount of energy absorbed and subsequently dissipated by those internalized materials.[33] While the intrinsic properties of plasmonic nanomaterials can be modulated by changing size, shape and composition, cell internalization can be enhanced by derivatizing their surface with specific biomolecules such as peptides,[34] carbohydrates[35] or proteins.[36] By tailoring the surface of these materials cell selectivity can be improved, which thereafter allows for a reduction in the NIR light-dose levels to values permitted by regulatory agencies. Clearly, one challenge in this area is being able to adjust the optical excitation to inflict apoptosis in treated areas only.

In this work we have used NPRs to efficiently and specifically induce apoptosis in transformed MEF cells by irradiating with an unfocused continuous wave NIR laser (1064 nm). More importantly, we have deciphered the molecular mechanism of apoptosis involved in this NPR-induced photothermal therapy, establishing the basis to predict the efficacy of this new treatment against cancer cells that are unresponsive to conventional chemotherapy or radiotherapy treatments.

RESULTS AND DISCUSSION

In general, *in vivo* or *in vitro* studies regarding photothermal treatment are based on the analysis of survival and tumor size/cell death, respectively.[13] Most studies use calcein as indicator of cell death[13,34,37] in conjunction with other fluorescence reporters that indicate loss of plasma membrane integrity including, but not limited to, ethidium homodimer-1,[38] ethidium bromide[39] and trypan blue.[40] It should be noted that loss of membrane integrity only occurs in necrotic cells.

Nevertheless, it is essential to note that for *in vitro* conditions, in the absence of phagocytic cells, late apoptotic cells also suffer from loss of membrane integrity (secondary necrosis), although this effect is observed later than during primary necrosis. Typically, the majority of photothermal therapy studies fail to discern between apoptotic and necrotic cell death, at least on a fundamental level. Thus, to truly unearth whether loss of cell viability is occurring by apoptosis or necrosis, a detailed kinetic study of phosfatidylserine (PS) translocation and membrane integrity as well as the molecular markers of apoptosis and the effect of its inhibition is mandatory.

A number of reports have shown that adjusting the intensity of radiation produces different outcomes (either apoptosis and necrosis) indiscriminately for both magnetothermal (magnetic hyperthermia)[41,42] and photothermal therapy.[40] Yet despite this, reports addressing the cellular response at biomolecular level remain elusive, *i.e.*, which pathway(s) are activated by photothermal therapy (*cf.* section Cell Death Mechanisms). In the following we address two of the most relevant and fundamental parameters concerning the photothermal response of cells containing NPRs, *i.e.*, kinetics and mechanisms.

Kinetics of Cell Death. The conduction electrons of metallic NPs can resonantly couple to the alternating electric field of electromagnetic radiation to produce a collective oscillation, a phenomenon refereed as localized surface plasmon resonance (LSPR). The optical properties of anisotropic AuNPs are largely affected by the symmetry axis and aspect ratio; the major contribution to the UV–vis–NIR spectrum of triangular gold nanoprisms (NPRs) corresponds to the in-plane dipolar mode located in the NIR range. The NPRs used in this study were synthesized to possess an LSPR band of *ca.* 1080 nm using a previously reported methodology (Figure 1A).[17] Their colloidal stability was maintained by attaching heterobifunctional 5 kDa polyethylene glycol (PEG) to the particle surface. The terminal carboxylic acid groups of the PEG facilitate subsequent biofunctionalization with aminated molecules through stable amide bonds. Glucose and a fluorophore (5-TAMRA-cadaverine or Alexa 647 depending on the application) were then conjugated to these stabilized NPRs to enhance cell uptake and provide fluorescent labeling, respectively (Figure 1B). Cells possess many carbohydrate receptors and different pathways for their internalization. Consequently, nanoparticles with conjugated carbohydrates are known to undergo enhanced cellular uptake. Furthermore, the presence of PEG and carbohydrates are known to prevent unspecific adsorption of proteins present in physiological media.[35] We opted for glucose based on our previous results.[17] Upon excitation by incident radiation of appropriate wavelength NPRs generate a sharp local heating by the photothermal

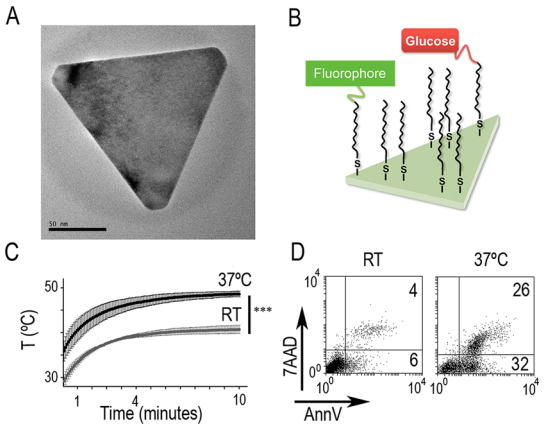

Figure 1. Triangular gold nanoprisms (NPRs) irradiated with a NIR laser (1064 nm) produce sharp heating effect which leads to cell death. (A) Transmission electron microscopy image of one NPR (scale bar: 50 nm). (B) Scheme of NPR functionalized with glucose for enhanced cell uptake and 5-TAMRA-cadaverine or Alexa 647 as a fluorescent marker (fluorophore). (C) Cells containing NPRs irradiated at room temperature (RT) and at 37 °C heated the surrounding medium to 41 and 50 °C respectively, corresponding to a temperature increase of 9 °C (* $p < 0.0001$) after less than 10 min irradiation time. (D) Cells containing NPRs were irradiated with NIR laser at RT or at 37 °C and cell death was analyzed 5 h later by monitoring AnnV staining and 7AAD incorporation by flow cytometry (FACS) on cells that had been irradiated for 10 min. RT irradiations produced a mere 10% cell death, whereas at 37 °C 58% cell death was observed.**

conversion of the absorbed light energy, rendering these particular particles as extremely efficient "nanoheaters". Since the manner of heating (*e.g.*, slow gradual *vs* fast heating, duration of the heat shock, *etc.*) can influence the response,[43] the temperature of the solution upon irradiation was monitored. Irradiating cells loaded with NPRs (cells were allowed to internalize NPRs overnight; *cf.* Materials and Methods) at room temperature with a Class IV continuous wave laser (1064 nm) for 10 min resulted in a rise in temperature from 29 to 41 °C ($\Delta T = 12$ °C); however, when cells were irradiated at 37 °C, a temperature more representative of cell environment *in vivo*, the temperature rose from 37 to 50 °C ($\Delta T = 13$ °C) (Figure 1C). This ΔT followed an initial very fast rise ($\Delta T > 5$ °C within the first minute, *ca.* 7 °C/min) followed by a saturation trend ($\Delta T < 1$ °C by 4 min) and in both cases, the rise in temperature resulting from NIR irradiation began to reach a plateau between 4 to 10 min. Although the rates of temperature rise were similar, the final temperature that could be achieved varied by almost 10 °C. Accordingly, preliminary *in vitro* studies were carried out to discern between the two possible chosen temperatures. Cells were incubated with NPRs and cell death was analyzed 5 h later by monitoring Annexin V (AnnV) staining and 7-Aminoactinomycin D (7AAD) incorporation in cells that had been irradiated for 10 min. AnnV is a protein that specifically binds to PS, a phospholipid that becomes exposed on the cell

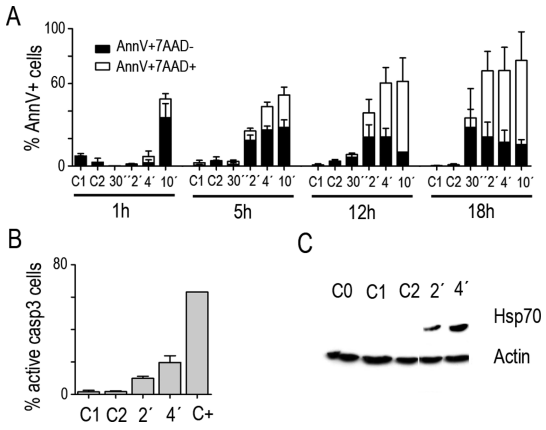

Figure 2. Irradiation of MEF cells loaded with NPRs induces apoptosis. MEF cells were incubated with glucose-modified nanoprisms (NPRs, 0.1 mg/mL) overnight and after washing out free NPRs they were irradiated by an unfocused continuous wave laser at 1064 nm for 30 s, 2, 4, or 10 min as indicated in Materials and Methods. (A and B) Necrotic and apoptotic features were analyzed by FACS (A) Annexin V (AnnV) and 7-Aminoactinomycin D (7AAD) were used as markers for apoptosis and necrosis, respectively at different time points after irradiation, *i.e.*, 1, 5, 12, and 18 h. (B) Caspase 3 activation was analyzed by FACS 5 h after cells were irradiated during 2 or 4 min as described in Materials and Methods. (C) The expression of heat shock proteins (Hsp70) in cells irradiated during 2 or 4 min was analyzed by Western blot. Actin served as loading control. C0: control cells. C1: control cells incubated with nanoparticles without irradiation. C2: control cells irradiated without nanoparticles. C+: cells incubated with staurosporine.

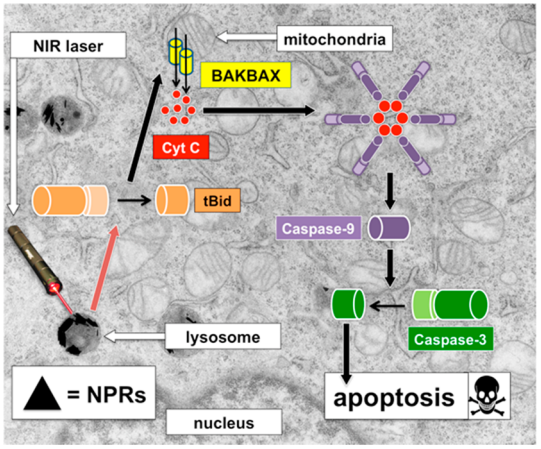

Scheme 1. Proposed mechanism of apoptosis resulting from NIR laser-irradiated MEF cells incubated with NPRs. MEF·wt cells incubated overnight with glucose modified NPRs (0.1 mg/mL) and irradiated with an unfocused laser beam for 4 min produce apoptosis *via* the activation of Bid. Activation of the pro-apoptotic BH3-only protein Bid leads to oligomerization of Bak and/or Bax in the outer mitochondrial membrane, which forms a pore allowing the release from the intermembrane space of molecules, including cytochrome c (cyt c). Cyt c in the cytoplasm, interacts with Apaf-1, dATP, and pro-caspase 9, forming a complex termed apoptosome that facilitates the activation of caspase 9 and consequently downstream executioner caspases-3, -6 or -7, which ultimately will be the responsible for apoptotic cell death.

surface as a result of apoptosis. 7AAD on the other hand is a fluorophore that intercalates with DNA and is used to analyze loss of membrane integrity during necrosis. The results clearly demonstrate how cells that were irradiated at RT were unable to reach sufficient temperatures to cause cell death (Figure 1D). At RT <10% cell death was observed; whereas cells irradiated at 37 °C produced 58% cell death. Consequently, all subsequent irradiation experiments were performed at 37 °C in order to mimic biological conditions, to produce the desired heating effect and to strive for reproducibility. It should be noted here that cells were seeded in 96-well plates and the diameter of the laser beam covers the entire well, thus, all cells were irradiated. In all experiments MEF cells were incubated with a concentration of NPRs of 100 μg/mL since at this concentration NPR uptake was maximum without any evidence of toxicity (Figure S1, Supporting Information).

As mentioned previously, in order to distinguish between apoptosis, primary necrosis and secondary necrosis, we have performed a detailed kinetic study on phosphatidylserine (PS) translocation and 7-Aminoactinomycin D (7AAD) uptake in MEF cells loaded with NPRs, after laser irradiation.

As shown in Figure 2A, MEFs irradiated for 30 s, 2 or 4 min did not show any sign of membrane disruption (7AAD−) or PS translocation (AnnV−) 1 h after the irradiation. This observation stands in contrast to other studies where cells die in less than 1 h with evident membrane rupture.[38] The percentage of both apoptotic (AnnV+7AAD−) and secondary necrotic (AnnV+7AAD+) cells clearly increased at longer incubation times (5, 12, and 18 h). However, it seems evident that cells become first apoptotic and only later the membrane is disrupted indicating that this is due to secondary necrosis. This indication is further supported by the following: (1) cells irradiated for just 30 s became exclusively apoptotic after 18 h, (2) cells irradiated for 10 min are mostly apoptotic after 1 h and secondary necrotic after 5 h, and (3) previous results showed that cells loaded with NPRs irradiated for 2 min with the same laser at higher intensity (30 W/cm^2) were necrotic immediately after irradiation.[17]

Altogether our data suggest that under the conditions used for these experiments cell death is driven by an apoptotic process, which ultimately gives rise to secondary necrosis. That is, cell death is apoptotic in origin and, moreover, these findings indicate that the extent of cell death can be regulated simply by modulating the time of irradiation (Figure 2A) and the mechanism of cell death is largely influenced by the intensity of irradiation.

To further confirm that cell death was apoptotic we analyzed activation of a specific apoptotic marker (caspase 3), 5 h after irradiation, the time point at which 50% cells were dead, mostly presenting an apoptotic phenotype (AnnV+7AAD−). The results regarding activation of caspase-3 (Figure 2B) mirror the previous results (Figure 2A). For instance, *ca.* 30% of cells

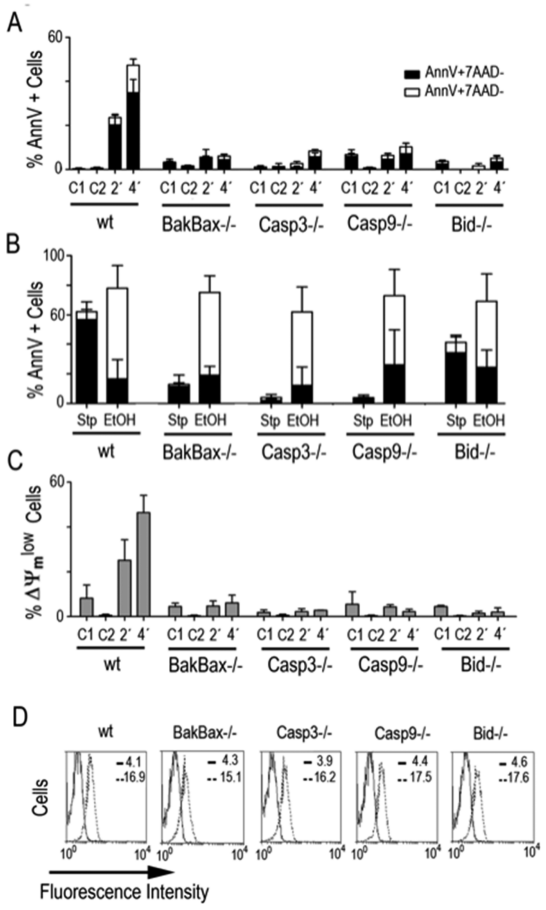

Figure 3. Analysis of the mitochondrial cell death pathways is involved in apoptosis induced by irradiation. MEF wild type cells (MEF·wt) or mutants lacking the Bcl-2 family members Bak and Bax (MEF·BakBax$^{-/-}$) and Bid (MEF·Bid$^{-/-}$) or the caspases, caspase 9 (MEF·Casp9$^{-/-}$) or caspase 3 (MEF·Casp3$^{-/-}$) were incubated with glucose-modified NPRs (0.1 mg/mL) overnight and irradiated by an unfocused laser beam either for 2 or 4 min as described in Materials and Methods. For control experiments cells were incubated with the apoptotic inductor staurosporine (stp) or the necrotic inductor ethanol (EtOH). Necrotic and apoptotic features were analyzed by FACS 5 h later. (A and B) Annexin V (AnnV) and 7-Aminoactinomycin D (7AAD). (C) loss of mitochondrial membrane potential ($\Delta\Psi_m$). (D) Cells were incubated with fluorescent-labeled NPRs overnight (discontinuous line) and the fluorescence intensity was measured by FACS. Note: continuous line represents cells without NPRs. C1: control cells incubated with NPRs without irradiation. C2: control cells irradiated without NPRs.

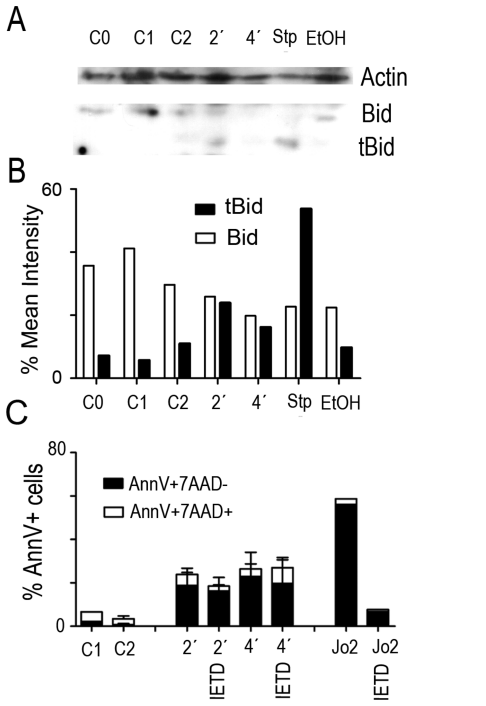

Figure 4. Bid is activated during irradiation of MEF·wt cells loaded with NPRs. (A) MEF wild type (wt) cells were incubated with NPRs (0.1 mg/mL) overnight and irradiated by an unfocused laser beam either for 2 or 4 min as described in Materials and Methods. As control cells were incubated with the apoptotic inductor staurosporine (Stp) or the necrotic inductor ethanol (EtOH). After 5 h, Bid activation was analyzed by immunoblot. Bid corresponds to the inactive form,whereas tBid is the active fragment. Actin served as loading control. (B) Bid and tBid were quantified by densitometry and normalized to the actin control. (C) Percentage of AnnV+ cells after 2 or 4 min of irradiation in the absence or presence of the caspase 8 inhibitor (IETD). The cytotoxic anti-Fas antibody Jo2 together with cycloheximide (CHX) was used as a control of caspase 8-mediated cell death. C0: cntrol cells. C1: control cells incubated with NPRs without irradiation. C2: control cells irradiated without NPRs.

irradiated for 4 min are positive for the active form of caspase-3, which corresponds to the number of apoptotic cells (AnnV+7AAD−) in Figure 2A. Both results therefore point to apoptosis as the mechanism of cell death using these conditions. Accordingly all subsequent experiments were based on analyzing different apoptotic features 5 h after irradiation for 2 and 4 min.

To confirm that cells loaded with NPRs were undergoing hyperthermia during irradiation we analyzed the expression of heat shock proteins (Hsp70s) by Western blot, *cf.* Figure 2C. These proteins are typically synthesized in response to heat stress in order to protect the cell for thermal or oxidative stress.[44] Figure 2C shows the dependence of the expression of Hsp70s as a function of irradiation time.

Cell Death Mechanisms. Our data indicate that photothermal treatment induces apoptosis in MEFs, when using suitable irradiation conditions. Next we analyzed the molecular mechanism of apoptosis involved in this process using these conditions (5 W/cm^2 for 2 or 4 min). There are two main pathways of apoptosis, *i.e.*, extrinsic and intrinsic pathways. The extrinsic pathway is triggered by mortal receptors when engaged by specific extracellular ligands usually expressed by cells from the immune system, which is an unlikely scenario to be triggered during photothermal therapy. The intrinsic pathway is characterized by mitochondrial outer-membrane permeabilization (MOMP) and caspase-3 activation regulated by the Bcl-2 family members as described in the introduction.

To analyze the involvement of this pathway during photothermal therapy induced by NPRs, we

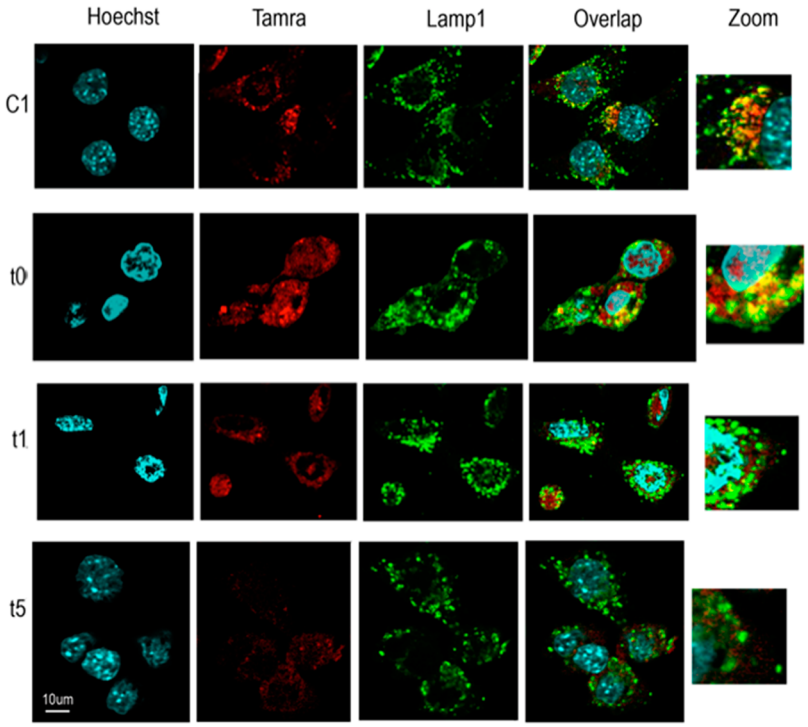

Figure 5. Localization of NPRs by confocal microscopy. MEF wild type (wt) cells were incubated with glucose- and TAMRA-modified NPRs (0.1 mg/mL) overnight and irradiated by an unfocused laser beam for 4 min as described in Materials and Methods. Cells were fixed with PFA 4% following irradiation (t_0), at 1 h (t_1) and at 5 h (t_5) later. In each case the cells were stained with Hoechst 3342 to stain DNA in nucleus, an anti-Lamp1 antibody as a lysosome marker followed by a secondary Alexa 488 labeled antibody. C1: control cells without irradiation. An enlargement of specific areas is shown in the right panels.

employed different mutant MEFs obtained from knockout (KO) mice, in which the pro-apoptotic proteins of the Bcl-2 family Bak and Bax (MEF·BakBax$^{-/-}$) and Bid (MEF·Bid$^{-/-}$) or the caspases, caspase 9 (MEF·Casp9$^{-/-}$) or caspase 3 (MEF·Casp3$^{-/-}$) have been deleted. Commensurate with the kinetic results summarized in Figure 2, Figure 3A shows that 5 h after irradiation, wild-type MEF cells (MEF·wt) suffer from apoptosis (AnnV+7AAD-). In contrast, MEF·BakBax$^{-/-}$, MEF·Bid$^{-/-}$, MEF·Casp9$^{-/-}$ and MEF·Casp3$^{-/-}$ were completely resistant to apoptosis and cell death induced after irradiation during both 2 and 4 min. As expected, apoptosis induced by staurosporine (a chemotherapy drug that activates the intrinsic mitochondrial pathway independently of Bid)[45] was completely blocked in MEF·BakBax$^{-/-}$, MEF·Casp9$^{-/-}$ and MEF·Casp3$^{-/-}$ cells, but not in MEF·Bid$^{-/-}$ cells. In contrast, necrotic cell death induced by ethanol was not affected by the absence of any pro-apoptotic protein (Figure 3B). Altogether, these results shown in Figure 3A and 3B undoubtedly confirm that cells are dying by apoptosis during photothermal treatment using NPRs. Otherwise mutant MEF cells would die by a process commensurate with that of the necrotic stimulus ethanol.

To further confirm the role of the mitochondria, mitochondrial damage following irradiation was investigated in wt and KO MEFs, monitoring loss of mitochondrial membrane potential ($\Delta\Psi_m$) by flow cytometry. As shown in Figure 3C, all of the KO MEFs maintained intact $\Delta\Psi_m$ after irradiation, whereas around 50% of MEF·wt irradiated during 4 min lost their $\Delta\Psi_m$. This result perfectly correlates with the percentage of cells undergoing apoptosis as monitored by AnnV staining (Figure 2A and 3A), supporting that mitochondria are involved in cell death execution.

The entry of fluorescent-labeled NPRs was similar in all mutant MEFs confirming that resistance to apoptosis and mitochondrial damage was not due to a reduced uptake of NPRs (Figure 3D). These results demonstrate the importance of the mitochondria and furthermore show that NPR-mediated photothermal therapy follows the intrinsic cell death pathway.

The resistance of all mutant MEF cells to apoptosis, cell death, and mitochondrial damage induced by NPR-mediated photothermal therapy indicates that the intrinsic mitochondrial pathway is activated by the BH3-only protein Bid. In this way Bid would lead to Bak and Bax activation, mitochondrial outer membrane permeabilisation, cytochrome C release and caspase-9 activation, which subsequently would lead to caspase-3 activation, apoptosis and cell death. The $\Delta\Psi_m$ loss resistance of MEF·Casp9$^{-/-}$ and MEF·Casp3$^{-/-}$ cells is not surprising, since it has been described that caspase-3 activation is required for a feedback amplification loop to completely and irreversibly disrupt $\Delta\Psi_m$.[46]

Our results suggest that the role of Bid is key to apoptosis induced by photothermal therapy and hence, the mechanism of Bid activation was investigated in detail. During apoptosis Bid is activated by proteolytic cleavage to generate the active truncated form tBid.[47] Then, tBid translocates into the mitochondria to induce the oligomerization of Bax and/or Bak and activate the intrinsic mitochondrial pathway of apoptosis. As shown in Figure 4A photothermal treatment induced the generation of tBid, which was more evident when cells were irradiated for 2 min as quantified by densitometry. The appearance of tBid was accompanied by a decrease in the amount of the Bid full protein form. As a control, apoptosis induced by staurosporine (Stp) was also accompanied by Bid processing into tBid, meanwhile necrosis induced by ethanol did not induce tBid as expected. The identity of the bands was confirmed by immunoblot using lysates from MEF·Bid$^{-/-}$ cells (data not shown).

Stp-induced apoptosis generates tBid from Bid; however, MEF·Bid$^{-/-}$ cells died at the same level as MEF-wt cells, meaning that Bid is dispensable for apoptosis induced by staurosporine.[48] Nevertheless, together with Figure 3A these results confirm the involvement of Bid in apoptosis induced by photothermal treatment using NPRs.

Our results show that Bid is activated during photothermal therapy. However, how this activation takes place remains unclear at this point. Bid is typically activated by caspase-8 during the extrinsic pathway of apoptosis triggered by death receptors.[47] In order to analyze if caspase-8 would be the mediator of Bid activation in our system, MEF·wt cells were treated with a caspase-8 inhibitor (IETD). As shown in Figure 5B, IETD failed to protect cells from NPR-induced photothermal therapy, thereby excluding caspase 8 as the upstream executor of Bid activation and cell death. IETD completely blocked cell death induced by the anti-Fas antibody Jo-2, which activates the extrinsic pathway and caspase-8 after binding to Fas, confirming the efficacy of IETD to block caspase 8 and cell death.

Although the process by which nanoheating of NPRs inside cells can activate Bid remains uncertain for the present work, we can hypothesize that lysosomal cathepsins released in the cytosol due to disruption of the lysosomes containing NPRs after photothermal treatment might cleave Bid as previously found for other stimuli.[49] We have found that fluorescent NPRs are located in the lysosome of MEF cells and are progressively released following 4 min of irradiation (Figure 5). In MEF cells loaded with NPRs before irradiation a colocalization (yellow-orange) between NPRs (red) and the lysosomal membrane protein marker Lamp-1 (green) can be observed (C1). Although some green fluorescence is still observed, all red NPRs are colocalizing with the lysosomes, indicating that all

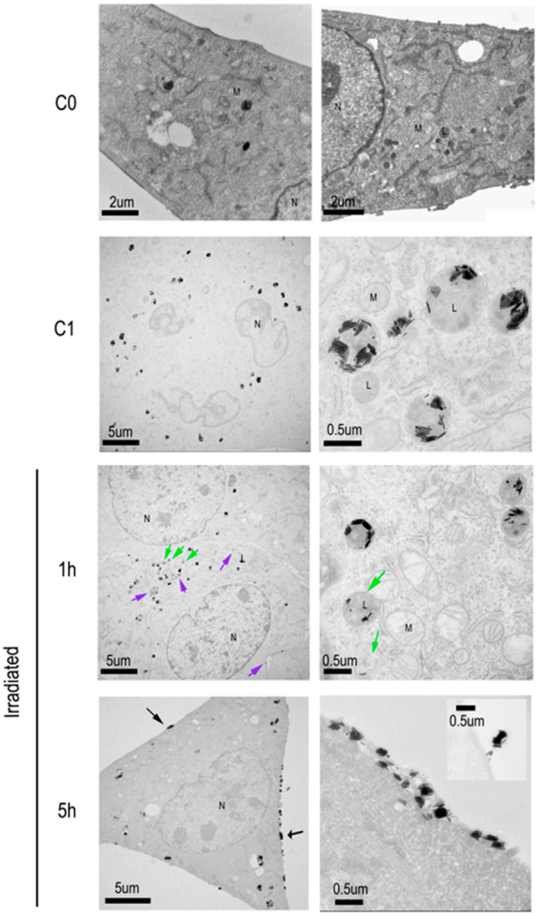

Figure 6. Localization of NPRs in MEF cells by TEM. MEF wild type (wt) cells were incubated with glucose modified NPRs (0.1 mg/mL) overnight and irradiated by an unfocused laser beam for 4 min as described in Materials and Methods. Cells were fixed with glutaraldehyde 1 h (t_1) and 5 h (t_5) after irradiation, embedded in resin and sliced with a diamond knife for inspection by TEM. Control experiments show NPRs within the lysosomes. One h after irradiation NPRs can still be observed in the lysosomes (green arrows), but there is a clear presence of the particles in the cytosol (violet arrows). Five h after irradiation very few NPRs remain in the lysosomes and can be observed embedded within the plasma membrane. C0: control cells. C1: control cells without irradiation. N: nucleus. M: mitochondria. L: lysosome.

NPRs are associated with these organelles. Immediately after irradiation (t_0) some NPRs were released (single red fluorescence), but there is still a significant amount of NPRs in the lysosomes (yellow). Progressively, the quantity of NPRs inside the lysosomes decreased and fluorescence diffused through the cytosol until 5 h of irradiation when almost no NPRs could be detected in lysosomes. These results indicate that irradiation causes release of NPRs from lysosomes, and that this release precedes cell death suggesting that lysosome permeabilization is involved in NPR-mediated cell death.

In order to confirm the NPR locations obtained from confocal microscopy data transmission electronic microscopy (TEM) was used to analyze the cellular location of the NPRs before and after release from

lysosomes. As shown in Figure 6, before irradiation the NPRs are stored exclusively in lysosomes of MEF cells (darkest endosomes); however, 1 h after irradiation significantly less NPRs are found in the lysosomes (green arrows), and some NPRs are even located in cell cytosol (violet arrows). The translocation of NPRs from lysosomes to cytosol is observed more clearly after 5 h, where very few NPRs remain associated with lysosomes. Further, the NPRs are clearly present in a lower concentration within the cell, which is commensurate with observations from confocal microscopy studies (Figure 5). Indeed TEM studies indicate that the majority of the NPRs are in fact being released from the cells, which explains the loss of fluorescence intensity observed by confocal microscopy and the appearance of NPRs aggregated in the medium as seen by conventional microscopy after irradiation (data not shown). From the combined TEM and confocal microscopy data we can conclude that following cell internalization NPRs are associated with lysosomes and after NIR irradiation they are released from the lysosomes, first into the cytosol before being released from the cell. Lysosomal permeabilization is needed for this release and other proteins from lysosomes such as cathepsins could be released with the NPRs. Although we have tried to specifically inhibit cathepsins in our model, the lack of efficacy of the inhibitors and/or their toxicity did not allow us to reach any clear conclusion.

Lysosomal leakage has been shown to initiate apoptosis induced by several stimuli.[50] Although extensive lysosomal rupture has been shown to induce necrosis, partial permeabilization may also be sufficient to induce caspase activation and MOMP.[51] A previous work reported that nanoparticles could be released from endosomes following photothermal treatment; however, this release had no effect on cell viability.[40] Lysosomal membrane permeabilization would lead to release of cathepsins into the cytosol, which would cleave and activate Bid as indicator for other stimuli,[49,52−55] although a formal proof of lysosomal involvement in cell death is still pending.

CONCLUSIONS

We have found that photothermal heating conditions of NPRs can be modulated to induce apoptotic cell death in transformed cells. Apoptosis is mediated by the intrinsic mitochondrial pathway initiated by Bid activation and completely dependent on caspase 3 activity, and is a more efficient and overall "cleaner" method of controlling cell death than necrosis. We want to emphasize the importance of ascertaining the mechanism of cell death induced by hyperthermia, not only to prevent secondary effects such as inflammation but also in order to avoid unsuccessful treatments. It is known that development of cancer as well as acquisition of drug resistance in tumoral cells is achieved by blocking certain cell death pathways. Therefore, understanding the mechanism of cell death following NP-induced photothermal therapy is crucial to predict and optimize the efficacy of this novel treatment against cancer cells that are unresponsive to conventional therapies.

MATERIALS AND METHODS

Synthesis of NPRs. Gold Nanoprisms stabilized with 5 kDa polyethylene glycol (PEG) and functionalized with 4-aminophenyl β-D-glucopyranoside (glucose) and/or 5-TAMRA cadaverine (tetramethylrhodamine-5-carboxamide cadaverine; absorption/emission = 545/576 nm) were synthesized according to the published literature procedures.[17] The functionalization with the dye was employed in the fluorescence microscopy study only.

Cell Culture. SV40-transformed murine embryonic fibroblasts (MEFs) were cultured in DMEM supplemented with 10% fetal bovine serum (FBS, PAN biotech) at 37 °C and 5% CO_2. MEF cells were used as a model to analyze the molecular mechanism of apoptosis since the next mutants were available: BakBax$^{-/-}$ SV40-transformed MEFs were generously provided by Dr. Christoph Borner (Institute of Molecular Medicine and Cell Research, Center for Biochemistry and Molecular Research, Freiburg, Germany),[56] and compared to a MEF wt cell line, generated by the same group. Casp9$^{-/-}$ and Casp3$^{-/-}$ SV40-transformed MEFs were generated and generously provided by the group of Richard A Flavell,[57] Bid$^{-/-}$ SV40-transformed MEFs were generated and generously provided by the laboratory of S. J. Korsmeyer.

Analysis of Pro-apoptotic Processes by Flow Cytometry. Cells were treated with 100 μg/mL NPRs overnight at 37 °C and 5% CO_2. After incubation cells were irradiated with a Ventus 1064 nm laser from Laser Quantum 5 W/cm^2 and incubated at 37 °C for different times 2−24 h. Subsequently, different apoptotic parameters were tested by FACS with a FACS Calibur instrument (BD Pharmingen) and CellQuests software as follows:

Nuclear, Cell Membrane, and Mitochondrial Membrane Perturbation. Phosphatidylserine (PS) exposure and 7-Aminoactinomycin D (7AAD) uptake were analyzed by FACS or fluorescence microscopy as described previously using annexin V−DY634 or FITC and 7AAD (Inmunostep).[58] Briefly, cells were incubated in 100 μL annexine binding buffer (ABB) with 1−1.5 μL annexine V and 1.5 μL 7AAD (inmunostep) for 15 min at room temperature. In some cases, the caspase 8 and 10 inhibitor IETD-fmk (Bachem; 30 μM) were added to cell cultures. $\Delta\psi_m$ was measured with the fluorescent probe 3,3′-dihexyloxacarbocyanine iodide (DiOC6; Invitrogen) 10 nM in 100 μL culture medium or ABB at 37 °C for 15 min.[59]

Caspase-3 Activation. Caspase-3 activation was analyzed by FACS as described previously.[58] Briefly cells were fixed with 1% paraformaldehyde (PFA) and incubated with a FITC-labeled monoclonal antibody (mAb) against the active form of caspase-3 (clone C92605; BD Pharmingen) diluted in 0.1% saponin in PBS. After two washes with 0.1% saponin in PBS, cells were resuspended in 1% PFA and analyzed by FACS.

Inmunoblot. 5 × 10^5 cells were washed in PBS and lysed in a buffer containing 1% Triton X-100 during 15 min on ice. Soluble protein fractions were recovered by centrifugation and separated by sodium dodecyl sulfate-polyacrylamide gel electrophoresis. Then, proteins were transferred to a PVDF membrane and blocked with 5% fat-free milk. The following primary antibodies (dilution) were incubated overnight at 4 °C: α-Bid (Goat, BD) (1/1000), Hsp70 (mouse, Stressgen (1/1000) or α-actin (Mouse, Sigma) (1/1000) as loading control, that was incubated for 1 h. Then, after a washing step and depending on the primary antibody used, blots were incubated during 1 h

at room temperature with secondary IgG antibodies conjugated with HRP (Sigma); α-mouse, α-rabbit at 1/20000 dilution or α-goat at 1/50000.

Analysis of Interaction of Nanoparticles—Cells. Cells were incubated with 100 μg/mL NPRs, which in addition to the glucose functionalization were functionalized with the dye Alexa 647, overnight at 37 °C and 5% CO_2. Subsequently NPR uptake was analyzed by FACS with a FACS Calibur instrument (BD Pharmingen) and CellQuests software.

Laser Setup and Temperature Measurement. For the NIR irradiation of cell heating experiments, a 1 W continuous wave Ventus laser (1064 nm, *ca.* 5 W/cm^2) supplied by Laser Quantum was coupled to a TEM_{00} fiber by means of fiber coupler (PAF-X-7-C from Thorlabs). Cells were incubated with NPRs overnight, after washing steps samples were positioned in front of the beam. The temperature of cell cultures was monitored in real time using a software developed by The University of Zaragoza using a thermocouple.

Confocal Microscopy. Cells grown on 6 mm diameter cover glasses were treated with 100 μg/mL of NPRs modified with glucose and TAMRA overnight. Cells were washed with PBS and fixed with 4% paraformaldehyde solution in phosphate buffered saline (PBS) for 20 min at 4 °C. Fixed cells were washed with 0.1% saponin in PBS, PBS and H_2O_d following the incubation with α-Lamp1 (rat, BD) (1/400) in PBS 0.1% saponin, 5% goat serum for 30 min at room temperature. After washing steps cells were incubated with the secondary antibody α-Rat-Alexafluor488 (goat, invitrogen) (1/500) 30 min at room temperature. Then were mounted on a drop of fluoromount-G (Southern Biotechnology Associates, Inc.) containing 2 μg/mL Hoechst 33342 (Invitrogen). Afterward, the cells were analyzed by confocal microscopy. Fluorescence images were taken at room temperature on a confocal microscope (Olympus FV10-i Oil Type), using the same settings for all the cell lines. The software FV10i-SW was used for minor adjustments to background and image overlay.

Transmission Electron Microscopy. For electron microscopy studies, cells were washed with PBS and subsequently fixed with 2.5% glutaraldehyde in 0.1 M phosphate buffer (PB) for 1 h at 4 °C. Then, the cells were washed with 0.1 M PB for four times. Sections were postfixed with 2% osmium, rinsed, dehydrated and embedded in Durcupan resin (Fluka, Sigma-Aldrich, St. Louis, USA). Semithin sections (1.5 μm) were cut with an Ultracut UC-6 (Leica, Heidelberg, Germany) and stained lightly with 1% toluidine blue. Finally, ultrathin sections (0.08 μm) were cut with a diamond knife, stained with lead citrate (Reynolds solution) and examined under a 200 kV transmission electron microscope FEI Tecnai TF20 (FEI Europe, Eindhoven, Netherlands).

Conflict of Interest: The authors declare no competing financial interest.

Acknowledgment. This work was supported by the MAT2011-26851-CO2-01, MAT2011-26851-CO2-02 and SAF2011-25390, projects of the Spanish Ministry of Science and Innovation, the grant ERC-Starting Grant 239931-NANOPUZZLE project and Fondo Social Europeo (FSE; Gobierno de Aragón). P.d.P., J.M.F., and J.P. thank ARAID for financial support, S.G.M. thanks Marie Curie Intra-European Fellowship 328985-COCOPOPS, and B.P. thanks the Alexander von Humboldt Foundation for a fellowship. Work from W.J.P. was supported by HSFP project RGP0052/2012

Supporting Information Available: UV—vis spectra of gold nanoprisms before and after functionalization with glucose and gold nanoprisms uptake and toxicity in MEF cells. This material is available free of charge *via* the Internet at http://pubs.acs.org.

REFERENCES AND NOTES

1. Lal, S.; Clare, S. E.; Halas, N. J. Nanoshell-Enabled Photothermal Cancer Therapy: Impending Clinical Impact. *Acc. Chem. Res.* **2008**, *41*, 1842–1851.
2. Kim, J.-W.; Galanzha, E. I.; Shashkov, E. V.; Moon, H.-M.; Zharov, V. P. Golden Carbon Nanotubes as Multimodal Photoacoustic and Photothermal High-contrast Molecular Agents. *Nat. Nanotechnol.* **2009**, *4*, 688–694.
3. Huschka, R.; Barhoumi, A.; Liu, Q.; Roth, J. A.; Ji, L.; Halas, N. J. Gene Silencing by Gold Nanoshell-Mediated Delivery and Laser-Triggered Release of Antisense Oligonucleotide and siRNA. *ACS Nano* **2012**, *6*, 7681–7691.
4. Munoz Javier, A.; del Pino, P.; Bedard, M. F.; Ho, D.; Skirtach, A. G.; Sukhorukov, G. B.; Plank, C.; Parak, W. J. Photoactivated Release of Cargo from the Cavity of Polyelectrolyte Capsules to the Cytosol of Cells. *Langmuir* **2008**, *24*, 12517–12520.
5. Boyer, D.; Tamarat, P.; Maali, A.; Orrit, M.; Lounis, B. Imaging Single Absorbing Nanoparticles in Cells by Photothermal Interference Contrast. *Biophys. J.* **2003**, *84*, 24A.
6. Baffou, G.; Bon, P.; Savatier, J.; Polleux, J.; Zhu, M.; Merlin, M.; Rigneault, H.; Monneret, S. Thermal Imaging of Nanostructures by Quantitative Optical Phase Analysis. *ACS Nano* **2012**, *6*, 2452–2458.
7. Bao, C.; Beziere, N.; del Pino, P.; Pelaz, B.; Estrada, G.; Tian, F.; Ntziachristos, V.; de la Fuente, J. M.; Cui, D. Gold Nanoprisms as Optoacoustic Signal Nanoamplifiers for *In Vivo* Bioimaging of Gastrointestinal Cancers. *Small* **2013**, *9*, 68–74.
8. Qin, Z. P.; Chan, W. C. W.; Boulware, D. R.; Akkin, T.; Butler, E. K.; Bischof, J. C. Significantly Improved Analytical Sensitivity of Lateral Flow Immunoassays by Using Thermal Contrast. *Angew. Chem. Int. Ed.* **2012**, *51*, 4358–4361.
9. Polo, E.; del Pino, P.; Pelaz, B.; Grazu, V.; de la Fuente, J. M. Plasmonic-driven Thermal Sensing: Ultralow Detection of Cancer Markers. *Chem. Commun.* **2013**, *49*, 3676–3678.
10. Wang, L. V.; Hu, S. Photoacoustic Tomography: *In Vivo* Imaging from Organelles to Organs. *Science* **2012**, *335*, 1458–1462.
11. Dreaden, E. C.; Mackey, M. A.; Huang, X. H.; Kang, B.; El-Sayed, M. A. Beating Cancer in Multiple Ways using Nanogold. *Chem. Soc. Rev.* **2011**, *40*, 3391–3404.
12. Weissleder, R. A Clearer Vision for *In Vivo* Imaging. *Nat. Biotechnol.* **2001**, *19*, 316–317.
13. Bardhan, R.; Lal, S.; Joshi, A.; Halas, N. J. Theranostic Nanoshells: From Probe Design to Imaging and Treatment of Cancer. *Acc. Chem. Res.* **2011**, *44*, 936–946.
14. Alkilany, A. M.; Thompson, L. B.; Boulos, S. P.; Sisco, P. N.; Murphy, C. J. Gold Nanorods: Their Potential for Photothermal Therapeutics and Drug Delivery, Tempered by the Complexity of their Biological Interactions. *Adv. Drug Deliv Rev.* **2012**, *64*, 190–199.
15. Chen, J.; Wang, D.; Xi, J.; Au, L.; Siekkinen, A.; Warsen, A.; Li, Z. Y.; Zhang, H.; Xia, Y.; Li, X. Immuno Gold Nanocages with Tailored Optical Properties for Targeted Photothermal Destruction of Cancer Cells. *Nano Lett.* **2007**, *7*, 1318–1322.
16. Baffou, G.; Girard, C.; Quidant, R. Mapping Heat Origin in Plasmonic Structures. *Phys. Rev. Lett.* **2010**, *104*, 136805(4).
17. Pelaz, B.; Grazu, V.; Ibarra, A.; Magen, C.; del Pino, P.; de la Fuente, J. M. Tailoring the Synthesis and Heating Ability of Gold Nanoprisms for Bioapplications. *Langmuir* **2012**, *28*, 8965–8970.
18. Bartczak, D.; Muskens, O. L.; Nitti, S.; Sanchez-Elsner, T.; Millar, T. M.; Kanaras, A. G. Interactions of Human Endothelial Cells with Gold Nanoparticles of Different Morphologies. *Small* **2012**, *8*, 122–130.
19. Mocan, T.; Matea, C. T.; Cojocaru, I.; Ilie, I.; Tabaran, F. A.; Zaharie, F.; Iancu, C.; Bartos, D.; Mocan, L. Photothermal Treatment of Human Pancreatic Cancer Using PEGylated Multi-Walled Carbon Nanotubes Induces Apoptosis by Triggering Mitochondrial Membrane Depolarization Mechanism. *J. Cancer* **2014**, *5*, 679–688.
20. Huang, X.; Kang, B.; Qian, W.; Mackey, M. A.; Chen, P. C.; Oyelere, A. K.; El-Sayed, I. H.; El-Sayed, M. A. Comparative Study of Photothermolysis of Cancer Cells with Nuclear-Targeted or Cytoplasm-Targeted Gold Nanospheres: Continuous Wave or Pulsed Lasers. *J. Biomed. Opt.* **2010**, *15*, 058002(7).
21. Li, J.-L.; Gu, M. Surface Plasmonic Gold Nanorods for Enhanced Two-Photon Microscopic Imaging and Apoptosis Induction of Cancer Cells. *Biomaterials* **2010**, *31*, 9492–9498.
22. Fernandez Cabada, T.; de Pablo, C. S.; Serrano, A. M.; Guerrero Fdel, P.; Olmedo, J. J.; Gomez, M. R. Induction of

Cell Death in a Glioblastoma Line by Hyperthermic Therapy based on Gold Nanorods. *Int. J. Nanomed.* **2012**, *7*, 1511–1523.
23. Bhatia, S. N.; von Maltzahn, G.; Park, J. H.; Agrawal, A.; Bandaru, N. K.; Das, S. K.; Sailor, M. J. Computationally Guided Photothermal Tumor Therapy Using Long-Circulating Gold Nanorod Antennas. *Cancer Res.* **2009**, *69*, 3892–3900.
24. Lowery, A. R.; Gobin, A. M.; Day, E. S.; Halas, N. J.; West, J. L. Immunonanoshells for Targeted Photothermal Ablation of Tumor Cells. *Int. J. Nanomed.* **2006**, *1*, 149–154.
25. Grivennikov, S. I.; Greten, F. R.; Karin, M. Immunity, Inflammation, and Cancer. *Cell* **2010**, *140*, 883–899.
26. Kerr, J. F.; Wyllie, A. H.; Currie, A. R. Apoptosis: a Basic Biological Phenomenon with Wide-ranging Implications in Tissue Kinetics. *Br. J. Cancer* **1972**, *26*, 239–257.
27. Ravichandran, K. S. Find-me and Eat-me Signals in Apoptotic Cell Clearance: Progress and Conundrums. *J. Exp. Med.* **2010**, *207*, 1807–1817.
28. Obeid, M.; Tesniere, A.; Ghiringhelli, F.; Fimia, G. M.; Apetoh, L.; Perfettini, J.-L.; Castedo, M.; Mignot, G.; Panaretakis, T.; Casares, N.; *et al.* Calreticulin Exposure Dictates the Immunogenicity of Cancer Cell Death. *Nat. Med.* **2007**, *13*, 54–61.
29. Groh, V.; Li, Y. Q.; Cioca, D.; Hunder, N. N.; Wang, W.; Riddell, S. R.; Yee, C.; Spies, T. Efficient Cross-priming of Tumor Antigen-specific T Cells by Dendritic Cells Sensitized with Diverse Anti-MICA Opsonized Tumor Cells. *Proc. Natl. Acad. Sci. U. S. A.* **2005**, *102*, 6461–6466.
30. Turk, B.; Stoka, V. Protease Signalling in Cell Death: Caspases *Versus* Cysteine Cathepsins. *FEBS Lett.* **2007**, *581*, 2761–2767.
31. Adams, J. M.; Cory, S. Bcl-2-regulated Apoptosis: Mechanism and Therapeutic Potential. *Curr. Opin. Immunol.* **2007**, *19*, 488–496.
32. Elmore, S. Apoptosis: A Review of Programmed Cell Death. *Toxicol. Pathol.* **2007**, *35*, 495–516.
33. Qin, Z.; Bischof, J. C. Thermophysical and Biological Responses of Gold Nanoparticle Laser Heating. *Chem. Soc. Rev.* **2012**, *41*, 1191–1217.
34. Yuan, H.; Fales, A. M.; Vo-Dinh, T. TAT Peptide-Functionalized Gold Nanostars: Enhanced Intracellular Delivery and Efficient NIR Photothermal Therapy Using Ultralow Irradiance. *J. Am. Chem. Soc.* **2012**, *134*, 11358–11361.
35. Moros, M.; Hernáez, B.; Garet, E.; Dias, J. T.; Sáez, B.; Grazu, V.; González-Fernández, A.; Alonso, C.; De La Fuente, J. M. Monosaccharides *Versus* PEG Functionalized NPs: Influence in the Cellular Uptake. *ACS Nano* **2012**, *6*, 1565–1577.
36. Ulbrich, K.; Hekmatara, T.; Herbert, E.; Kreuter, J. Transferrin- and Transferrin-receptor Antibody-modified Nanoparticles Enable Drug Delivery Across the Blood-brain Barrier (BBB). *Eur. J. Pharm. Biopharm.* **2009**, *71*, 251–256.
37. Loo, C.; Lowery, A.; Halas, N. J.; West, J.; Drezek, R. Immunotargeted Nanoshells for Integrated Cancer Imaging and Therapy. *Nano Lett.* **2005**, *5*, 709–711.
38. Day, E. S.; Bickford, L. R.; Slater, J. H.; Riggall, N. S.; Drezek, R. A.; West, J. L. Antibody-conjugated Gold-gold Sulfide Nanoparticles as Multifunctional Agents for Imaging and Therapy of Breast Cancer. *Int. J. Nanomed.* **2010**, *5*, 445–454.
39. Huff, T. B.; Tong, L.; Zhao, Y.; Hansen, M. N.; Cheng, J. X.; Wei, A. Hyperthermic Effects of Gold Nanorods on Tumor Cells. *Nanomedicine* **2007**, *2*, 125–132.
40. Krpetic, Z.; Nativo, P.; See, V.; Prior, I. A.; Brust, M.; Volk, M. Inflicting Controlled Nonthermal Damage to Subcellular Structures by Laser-Activated Gold Nanoparticles. *Nano Lett.* **2010**, *10*, 4549–4554.
41. Gilchrist, R. K.; Medal, R.; Shorey, W. D.; Hanselman, R. C.; Parrott, J. C.; Taylor, C. B. Selective Inductive Heating of Lymph Nodes. *Ann. Surg.* **1957**, *146*, 596–606.
42. Bae, K. H.; Park, M.; Do, M. J.; Lee, N.; Ryu, J. H.; Kim, G. W.; Kim, C.; Park, T. G.; Hyeon, T. Chitosan Oligosaccharide-Stabilized Ferrimagnetic Iron Oxide Nanocubes for Magnetically Modulated Cancer Hyperthermia. *ACS Nano* **2012**, *6*, 5266–5273.
43. Szymańska, Z.; Zylicz, M. Mathematical Modeling of Heat Shock Protein Synthesis in Response to Temperature Change. *J. Theor. Biol.* **2009**, *259*, 562–569.
44. Helmbrecht, K.; Zeise, E.; Rensing, L. Chaperones in Cell Cycle Regulation and Mitogenic Signal Transduction: a Review. *Cell. Proliferation* **2000**, *33*, 341–65.
45. Wei, M. C.; Zong, W. X.; Cheng, E. H. Y.; Lindsten, T.; Panoutsakopoulou, V.; Ross, A. J.; Roth, K. A.; MacCregor, G. R.; Thompson, C. B.; Korsmeyer, S. J. Proapoptotic BAX and BAK: A Requisite Gateway to Mitochondrial Dysfunction and Death. *Science* **2001**, *292*, 727–730.
46. Ricci, J.-E.; Gottlieb, R. A.; Green, D. R. Caspase-Mediated Loss of Mitochondrial Function and Generation of Reactive Oxygen Species during Apoptosis. *J. Cell Biol.* **2003**, *160*, 65–75.
47. Li, H.; Zhu, H.; Xu, C.-j.; Yuan, J. Cleavage of BID by Caspase 8 Mediates the Mitochondrial Damage in the Fas Pathway of Apoptosis. *Cell* **1998**, *94*, 491–501.
48. Ren, D.; Tu, H.-C.; Kim, H.; Wang, G. X.; Bean, G. R.; Takeuchi, O.; Jeffers, J. R.; Zambetti, G. P.; Hsieh, J. J. D.; Cheng, E. H. Y. BID, BIM, and PUMA Are Essential for Activation of the BAX- and BAK-Dependent Cell Death Program. *Science* **2010**, *330*, 1390–1393.
49. Cirman, T.; Orešić, K.; Mazovec, G. D.; Turk, V.; Reed, J. C.; Myers, R. M.; Salvesen, G. S.; Turk, B. Selective Disruption of Lysosomes in HeLa Cells Triggers Apoptosis Mediated by Cleavage of Bid by Multiple Papain-like Lysosomal Cathepsins. *J. Biol. Chem.* **2004**, *279*, 3578–3587.
50. Boya, P.; Kroemer, G. Lysosomal Membrane Permeabilization in Cell Death. *Oncogene* **2008**, *27*, 6434–6451.
51. KÅGedal, K.; Johansson, U. N. O.; ÖLlinger, K. The Lysosomal Protease Cathepsin D Mediates Apoptosis Induced by Oxidative Stress. *FASEB J.* **2001**, *15*, 1592–1594.
52. Foghsgaard, L.; Wissing, D.; Mauch, D.; Lademann, U.; Bastholm, L.; Boes, M.; Elling, F.; Leist, M.; Jäättelä, M. Cathepsin B Acts as a Dominant Execution Protease in Tumor Cell Apoptosis Induced by Tumor Necrosis Factor. *J. Cell Biol.* **2001**, *153*, 999–1010.
53. Brunk, U. T.; Svensson, I. Oxidative Stress, Growth Factor Starvation and Fas Activation May All Cause Apoptosis Through Lysosomal Leak. *Redox Rep.* **1999**, *4*, 3–11.
54. Yuan, X.-M.; Li, W.; Dalen, H.; Lotem, J.; Kama, R.; Sachs, L.; Brunk, U. T. Lysosomal Destabilization in p53-induced Apoptosis. *Proc. Natl. Acad. Sci. U. S. A.* **2002**, *99*, 6286–6291.
55. Zang, Y.; Beard, R. L.; Chandraratna, R. A.; Kang, J. X. Evidence of a Lysosomal Pathway for Apoptosis Induced by the Synthetic Retinoid CD437 in Human Leukemia HL-60 Cells. *Cell Death Differ.* **2001**, *8*, 477–485.
56. Wei, M. C.; Zong, W. X.; Cheng, E. H.; Lindsten, T.; Panoutsakopoulou, V.; Ross, A. J.; Roth, K. A.; MacGregor, G. R.; Thompson, C. B.; Korsmeyer, S. J. Proapoptotic BAX and BAK: a Requisite Gateway to Mitochondrial Dysfunction and Death. *Science* **2001**, *292*, 727–30.
57. Lakhani, S. A.; Masud, A.; Kuida, K.; Porter, G. A.; Booth, C. J.; Mehal, W. Z.; Inayat, I.; Flavell, R. A. Caspases 3 and 7: Key Mediators of Mitochondrial Events of Apoptosis. *Science* **2006**, *311*, 847–851.
58. Pardo, J.; Bosque, A.; Brehm, R.; Wallich, R.; Naval, J.; Mullbacher, A.; Anel, A.; Simon, M. M. Apoptotic Pathways are Selectively Activated by Granzyme A and/or Granzyme B in CTL-mediated Target Cell Lysis. *J. Cell Biol.* **2004**, *167*, 457–68.
59. Aporta, A.; Arbues, A.; Aguilo, J. I.; Monzon, M.; Badiola, J. J.; de Martino, A.; Ferrer, N.; Marinova, D.; Anel, A.; Martin, C.; *et al.* Attenuated *Mycobacterium tuberculosis* SO2 Vaccine Candidate Is Unable to Induce Cell Death. *PLoS One* **2012**, *7*, e45213.